IET Nanobiotechnology

IET The Institution of Engineering and Technology WILEY

ORIGINAL RESEARCH PAPER

Metabolomic profiling of ZrO$_2$ nanoparticles in MC3T3-E1 cells

Mingfu Ye[1] (ORCID) | Linhu Wang[2] | Zhang Wu[3] | Wenjun Liu[1]

[1]Department of Oral Implantology, Stomatological Hospital of Xiamen Medical College, Xiamen Key Laboratory of Stomatological Disease Diagnosis and Treatment, Xiamen, China

[2]Department of Stomatology, General Hospital of Central Theater Command, Wuhan, China

[3]Department of Prosthodontics, Stomatological Hospital of Xiamen Medical College, Xiamen Key Laboratory of Stomatological Disease Diagnosis and Treatment, Xiamen, China

Correspondence

Mingfu Ye, Department of Oral Implantology, Stomatological Hospital of Xiamen Medical College, Xiamen Key Laboratory of Stomatological Disease Diagnosis and Treatment, No. 1309 Lvling Road, Xiamen 361008, Fujian, China.
Email: dentist_yipmyonphu@163.com

Abstract

The authors' previous study showed that zirconium oxide nanoparticles (ZrO$_2$ NPs) induce toxic effects in MC3T3-E1 cells; however, its toxicological mechanism is still unclear. Liquid chromatography–mass spectrometry/time-of-flight mass spectrometry was used to reveal the metabolite profile and toxicological mechanism of MC3T3-E1 cells in response to ZrO$_2$ NPs. The results demonstrated that MC3T3-E1 cells treated with ZrO$_2$ NPs for 24 and 48 h presented different metabolic characteristics. Following ZrO$_2$ NP treatment for 24 h, 96 upregulated and 129 downregulated metabolites in the positive ion mode, as well as 91 upregulated and 326 downregulated metabolites in the negative ion mode were identified. Following ZrO$_2$ NP treatment for 48 h, 33 upregulated and 174 downregulated metabolites were identified in the positive ion mode, whereas 37 upregulated and 302 downregulated metabolites were confirmed in the negative ion mode. Among them, 42 differential metabolites were recognised as potential metabolites contributing to the induced toxic effects of ZrO$_2$ NPs in MC3T3-E1 cells. Most of the differential metabolites were lysophosphatidylcholine and lysophosphatidylethanolamide, indicating that exposure to ZrO$_2$ NPs may have a profound impact on human cellular function by impairing the membrane system. The results also provide new clues for the toxicological mechanism of ZrO$_2$ NP dental materials.

KEYWORDS
biomarkers, lysoPCs, lysoPEs, metabolite profiling, ZrO$_2$ nanoparticles

1 | INTRODUCTION

Zirconium oxide (ZrO$_2$) is one of the most widely used metal compounds due to its high mechanical strength and low toxicity [1]. ZrO$_2$ nanoparticles (NPs) have been commercialised for medical applications, mostly medical devices, owing to their biocompatibility and resistance to biocorrosion [2]. Recently, the toxicity of NPs has been reported, which has led to reduce its medical use [3]. The underlying mechanisms of metal NP toxicity include oxidative stress, inflammation, immunotoxicity, and genotoxicity [4]. Successful ZrO$_2$ dental implants rely on three main components: bone, connective tissue, and epithelium. Hard tissue plays an important role in the implant, occupying one-third of the height of the implant, while bone tissue contacts the surface of the implant with an appropriate biological width to form complete osseointegration. Our previous studies have revealed that MC3T3-E1 cells treated with 100 μg/ml ZrO$_2$ NPs decreased in size and lost their normal morphology, thereby indicating that NPs damaged

the cytoskeleton system. Thus, MC3T3-E1 cells function as a model for toxicity analysis of ZrO$_2$ NPs (Ye and Shi, 2018). NPs induce autophagy by activating mitogen-activated protein kinase ERK1/2 (p44/p42) [5]. Previous studies have suggested that multivesicular bodies that intake ZrO$_2$ NPs experience increased levels of mitochondrial reactive oxygen species (ROS) levels, which further activate inflammasomes; thus, providing a crucial link between oxidative stress and inflammation in ZrO$_2$ NP toxicity [6–8]. However, biomarkers for the accurate diagnosis of ZrO$_2$ NP toxicity are still lacking.

Metabolomics, as a quantitative assessment of endogenous small molecule metabolites within a biological system, has been used successfully to discover biomarkers for a variety of diseases, including NP-induced toxicity [9, 10]. Metabolomic studies have shown that gold NPs induce metabolic alterations in human hepatocellular carcinoma (HepG2) cells, and citrate-modified silver NPs cause abnormality in purine metabolism, amino acid metabolism, and glycine metabolism [11, 12]. Considered together, the metabolomic studies indicate that

NPs stimulate metabolic machineries to produce different metabolites and provide an experimental basis for exploring the toxicity mechanism of NPs. Nanoparticles may directly interact with proteins, lipids, and DNA, which result in protein degradation, membrane damage, and mutagenesis. Therefore, metabolomics may provide new insights into the mechanisms underlying NP toxicity [6]. Studying the alteration of metabolic profiles following exposure to ZrO_2 NPs can identify metabolic alterations, which is critical for detecting the toxic effects of ZrO_2 NPs. Understanding the toxicological mechanism of ZrO_2 NPs can provide new evidence that will lead to new methods for improving ZrO_2 NP dental materials.

Our previous studies have revealed the characteristics of ZrO_2 NPs (size: 31.9 ± 1.9 nm; particle dispersion index: 0.328; charge: 42.4 ± 7.4 mV; morphology: small rod-shaped spheres) and toxicity of ZrO_2 NPs against MC3T3-E1 cells (IC50 100 µg/ml), and also found that ZrO_2 NPs damages MC3T3-E1 cells through oxidative stress, inflammation, and altered immunity [13]. To further explore the toxicological mechanism, we performed a non-targetted metabolomic analysis to profile metabolite changes when MC3T3-E1 cells have been exposed to ZrO_2 NPs, which provided new clues for the toxicological mechanism and further study.

2 | MATERIALS AND METHODS

2.1 | Construction of a ZrO_2 NPs-induced MC3T3-E1 cell injury model

MC3T3-E1 cells were purchased from the Cell Bank of the Chinese Academy of Sciences and were cultured in an alpha minimum essential medium with ribonucleosides, deoxyribonucleosides, 2 mM L-glutamine, and 1 mM sodium pyruvate, without ascorbic acid (Catalogue No. A1049001, GIBCO) and supplemented with 10% foetal bovine serum (GIBCO) at 37°C, and 5% CO_2. The cells were incubated with ZrO_2 NPs to induce cellular injury. As previously described, the stock solution of ZrO_2 NPs was prepared as follows: ZrO_2 NPs (CAS 544760, Sigma) were dissolved in a phosphate buffer solution (CAS P1022, Solarbio) and shaken with an ultrasonic crushing system for 30 min on ice to prepare a 500 µg/ml stock solution. This stock solution was diluted to 100 µg/ml with a complete medium for further experiments [13]. The MC3T3-E1 cells treated with 100 µg/ml ZrO_2 NPs were divided into four groups: MC3T3-E1 cells with the mock treatment for 24 h as Group A; MC3T3-E1 cells with ZrO_2 NPs for 24 h as Group B; MC3T3-E1 cells with the mock treatment for 48 h as Group C; and MC3T3-E1 with ZrO_2 NPs for 48 h as Group D. The experiments in each group were performed in 12 replicates.

2.2 | Cell extraction for metabolite profiling

The cells were collected, resuspended in 50% methanol buffer (CAS M116115, Aladdin), vortexed for 1 min, incubated at room temperature for 10 min, and then incubated overnight at −20°C. Supernatants of the cell extracts were transferred to a 96-well plate after centrifugation at 4000 g for 20 min. The samples were stored at −80°C until liquid chromatography–mass spectrometry/time-of-flight (LC-MS/Q-TOF) mass spectrometry (MS) analysis. Quality control (QC) samples were prepared by combining 10 µl of each extraction [14].

2.3 | LC-MS/Q-TOF experiments

An ACQUITY UPLC T3 column (100 mm × 2.1 mm, 1.8 µm, Waters) was used for reversed-phase separation on an ExionLC system (SCIEX). The mobile phase consisted of Solvent A (0.1% formic acid in H_2O) and Solvent B (0.1% formic acid in acetonitrile). The flow rate was 0.4 ml/min; the oven temperature was set to 35°C; and the injection volume was 4 µl. The elution conditions were as follows: 0–0.5 min, 5% B; 0.5–7 min, 5%–100% B; 7–8 min, 100% B; 8–8.1 min, 100% to 5% B; and 8.1–10 min, 5% B.

A high-resolution tandem mass spectrometer Triple-TOF5600plus (SCIEX) was used to detect metabolites in both positive and negative ion modes. The curtain gas was set to 30 pounds per square inch (PSI); ion source gas1 was set to 60 PSI; ion source gas2 was set to 60 PSI; and an interface heater temperature was set to 650°C. The ion spray voltage floating was set to 5000 and −4500 V for positive and negative ion modes, respectively. We obtained the mass spectra data in information dependent acquisition mode, with a TOF mass ranging from 60 to 1200 Da. The total cycle time was fixed to 0.56 s. The mass accuracy was calibrated every 20 samples, and a QC sample was acquired after every 10 samples.

2.4 | Bioinformatics analysis of the untargetted metabolomic dataset

The acquired MS data pretreatments, including peak picking, peak grouping, retention time (RT) correction, second peak grouping, and annotation of isotopes and adducts, were performed using the XCMS software. Liquid chromatography–mass spectrometry raw data files were converted into mzXML format and then processed by XCMS, CAMERA, and metaX [15] toolboxes implemented with the R software. Each ion was identified by combining the RT and m/z data. The intensities of each peak were recorded, and a three-dimensional matrix containing arbitrarily assigned peak indices (RT-m/z pairs), sample names (observations), and ion intensity information (variables) was generated.

The online Kyoto Encyclopedia of Genes and Genomes (KEGG) database and the Human Metabolome Database (HMDB) were used to annotate the metabolites by matching the exact molecular mass data (m/z) of samples with those from the database. If a mass difference between the observed and database values was less than 10 ppm, the metabolite would be annotated, and the molecular formula for metabolites would be identified and validated by the isotopic distribution measurements. We also used an in-house fragment spectrum library of metabolites to validate the metabolite identification.
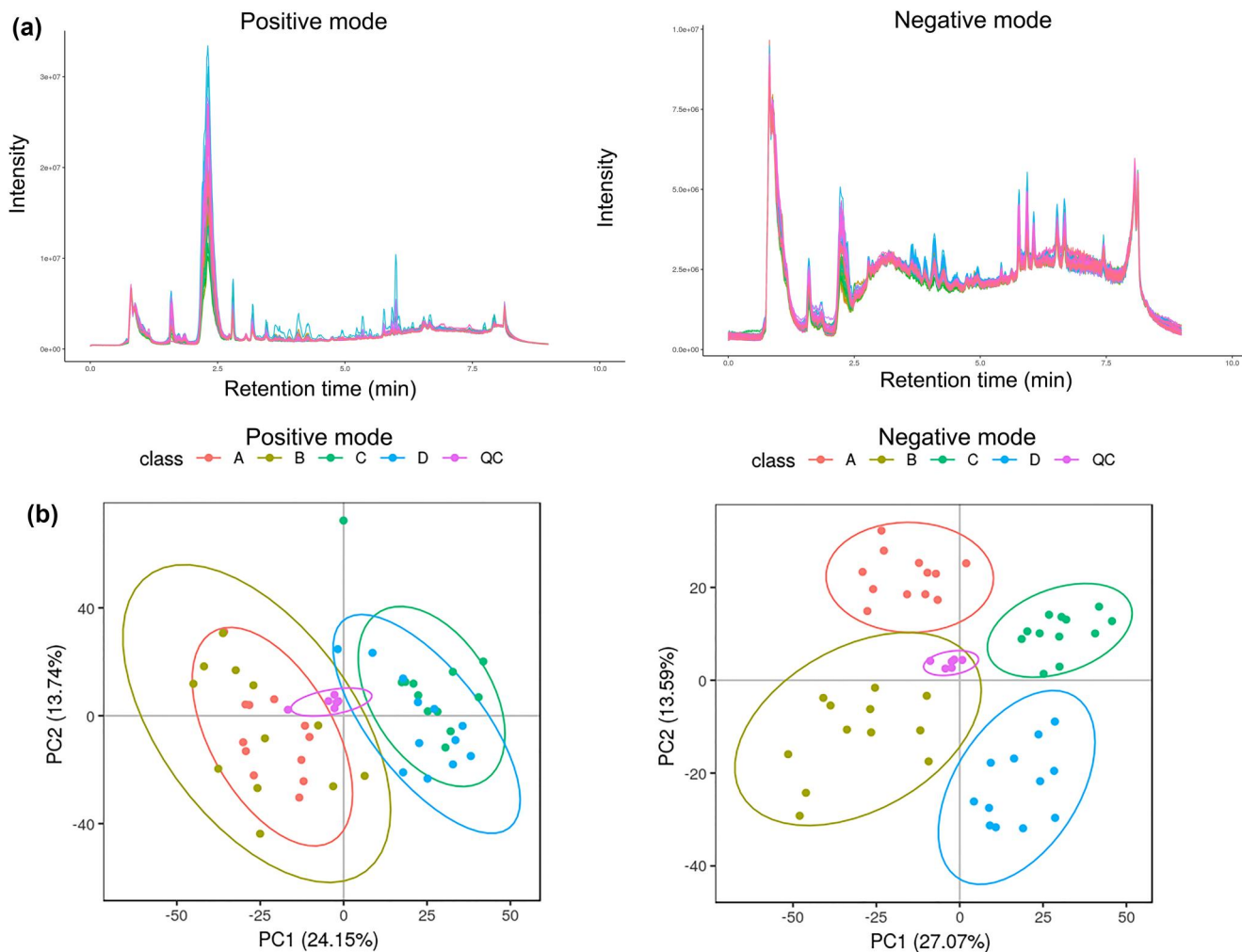
FIGURE 1 Quality control (QC) of metabolomic analysis using the liquid chromatography–mass spectrometry/time-of-flight mass spectrometry system. (a) Total ion chromatograms in the positive and negative ion modes. The peak retention time and peak area of the QC samples overlap well; (b) Unsupervised principal component analysis results in the positive and negative ion modes. QC samples are tightly packed together, indicating that the quality of the samples is high

The intensity of the peak data was further preprocessed by metaX [15] Those features that were detected in less than 50% of the QC samples or 80% of biological samples were removed, and the remaining peaks with missing values were imputed with the k-nearest neighbour algorithm to further improve the data quality. A principal component analysis (PCA) was performed for outlier detection and evaluation of the batch effects was performed using a preprocessed dataset. QC-based robust LOcally WEighted Scatter-plot Smoother signal correction was fitted to the QC data considering the order of injection to minimise the signal intensity drift over time. Furthermore, the relative standard deviations of the metabolic features were calculated across all QC samples, and those >30% were removed.

2.5 | Statistical analysis

Student's t-test was conducted to detect differences in the metabolite concentrations between the two groups. The p-value was adjusted for multiple tests using the false discovery rate method (Benjamini–Hochberg). Supervised partial least squares-discriminant analysis partial least squares discriminant analysis (PLS-DA) was conducted through metaX to discriminate the different variables between groups. The variable importance for projection (VIP) score was calculated. A VIP cut-off score of 1.0 was used to select important features.

3 | RESULTS

3.1 | Overview of metabolic profiling

To investigate the metabolic profiling of ZrO_2 NPs on MC3T3-E1 cells, four groups were used: Group A is MC3T3-E1 cells with mock treatment for 24 h; Group B is MC3T3-E1 cells with ZrO_2 NPs for 24 h; Group C is MC3T3-E1 cells with mock treatment for 48 h; and Group D is MC3T3-E1 cells with ZrO_2 NPs for 48 h. The total ion chromatograms of samples in the positive and negative ion modes were used to assess the quality of metabolomic data (Figure 1a). A good overlap of the
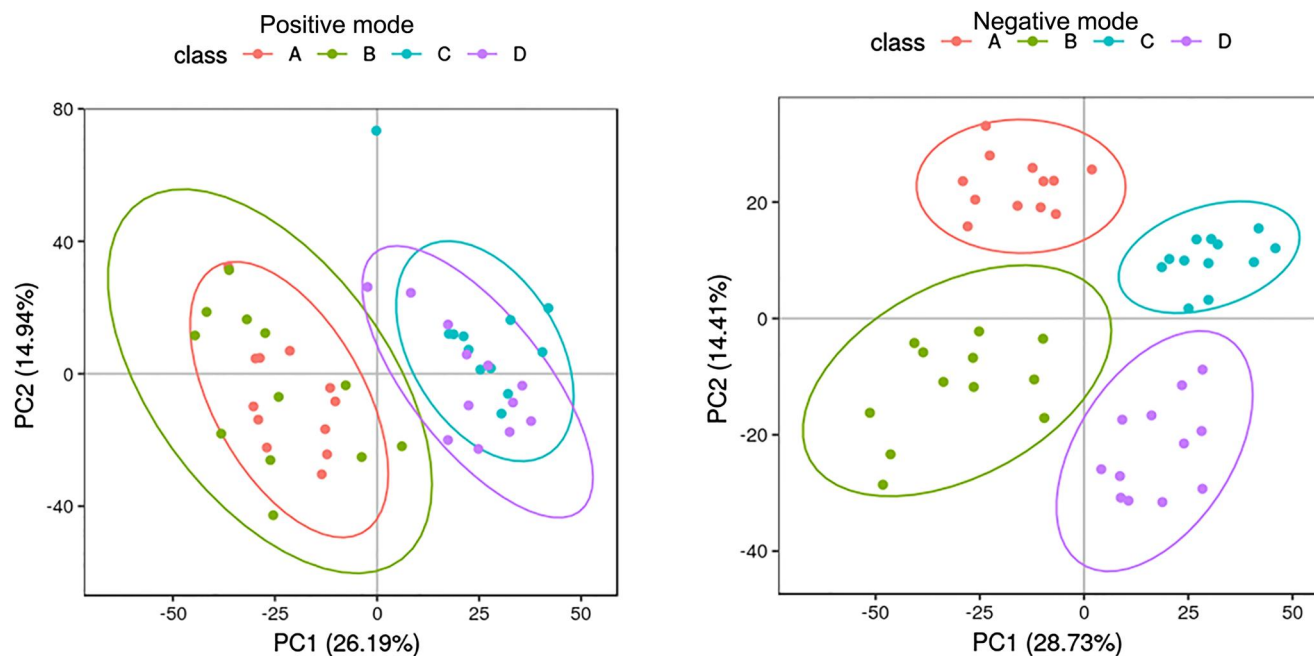
FIGURE 2 Metabolomic profiles of the zirconium oxide nanoparticles-treated and control groups. The outline view of all samples shows the principal component analysis scores for both the positive and negative ion modes

chromatograms for all samples in the positive or negative ion mode confirmed the RT, reproducibility, and stability of the instrument (Figure 1a). Moreover, we observed differences in the peak intensities between the metabolic profiles of MC3T3-E1 cells treated by ZrO_2 NPs for 24 and 48 h and those of the QC samples. Quality control samples in the principle component analysis were tightly packed, which indicated that the quality of the QC samples was high (Figure 1b).

3.2 | Normalisation and multivariate statistical analysis

First, we analysed the difference in the global metabolite between the ZrO_2 NPs-treated and control groups. PCA models were then used to analyse the metabolic changes; the PCA score plots showed that the samples from the ZrO_2 NPs-treated and control groups indicated consistent classification and significant separation in the negative ion mode, with 43.14% of the total variance in the data represented by the first two principal components (Figure 2). There were different metabolic characteristics in the positive ion mode; those plots revealed that the cellular metabolite of the ZrO_2 NPs-treated group changed significantly in the negative ion mode.

3.3 | Identification of differential metabolites

MetaX was used to identify metabolites. The results indicated that among the total of 7603 metabolites detected in the

positive ion mode, 5142 were high-quality metabolites; among the total of 7194 metabolites detected in the negative ion mode, 4964 were high-quality metabolites. Those high-quality features were collected for subsequent statistical analysis. A cluster analysis showed that these high-quality metabolites are primarily molecules related to lipid metabolism and organic acids and their derivatives. Notably, the number of unidentifiable metabolites in the negative ion mode was higher than that in the positive ion mode (Figure 3a).

The metabolic differences between the ZrO_2 NPs-treated and control groups were profiled. First, the variables with VIP value >1 had a good correlation with separation, which applies to the candidate list. Those metabolites were further subjected to a fold change (FC) analysis and Student's t-test with Benjamini–Hochberg correction to identify the differential metabolites. As shown in Table 1, 96 upregulated and 129 downregulated metabolites were identified in the positive ion mode at 24 h following ZrO_2 NP treatment; 91 upregulated and 326 downregulated metabolites were identified in the negative ion mode at 24 h following ZrO_2 NP treatment; 33 upregulated and 174 downregulated metabolites were identified in the positive ion mode at 48 h following ZrO_2 NP treatment; and 37 upregulated and 302 downregulated metabolites were identified in the negative ion mode at 48 h following ZrO_2 NP treatment. A hierarchical clustering analysis was performed to demonstrate the global overview of all differential metabolites that were visualised (Figure 3b,c). The results show that the abundance of metabolites was significantly different between the ZrO_2 NP and control groups at 24 and 48 h, in positive and negative ion modes.

(a)

Positive mode

Negative mode

(b)

Positive mode

Negative mode

(c)

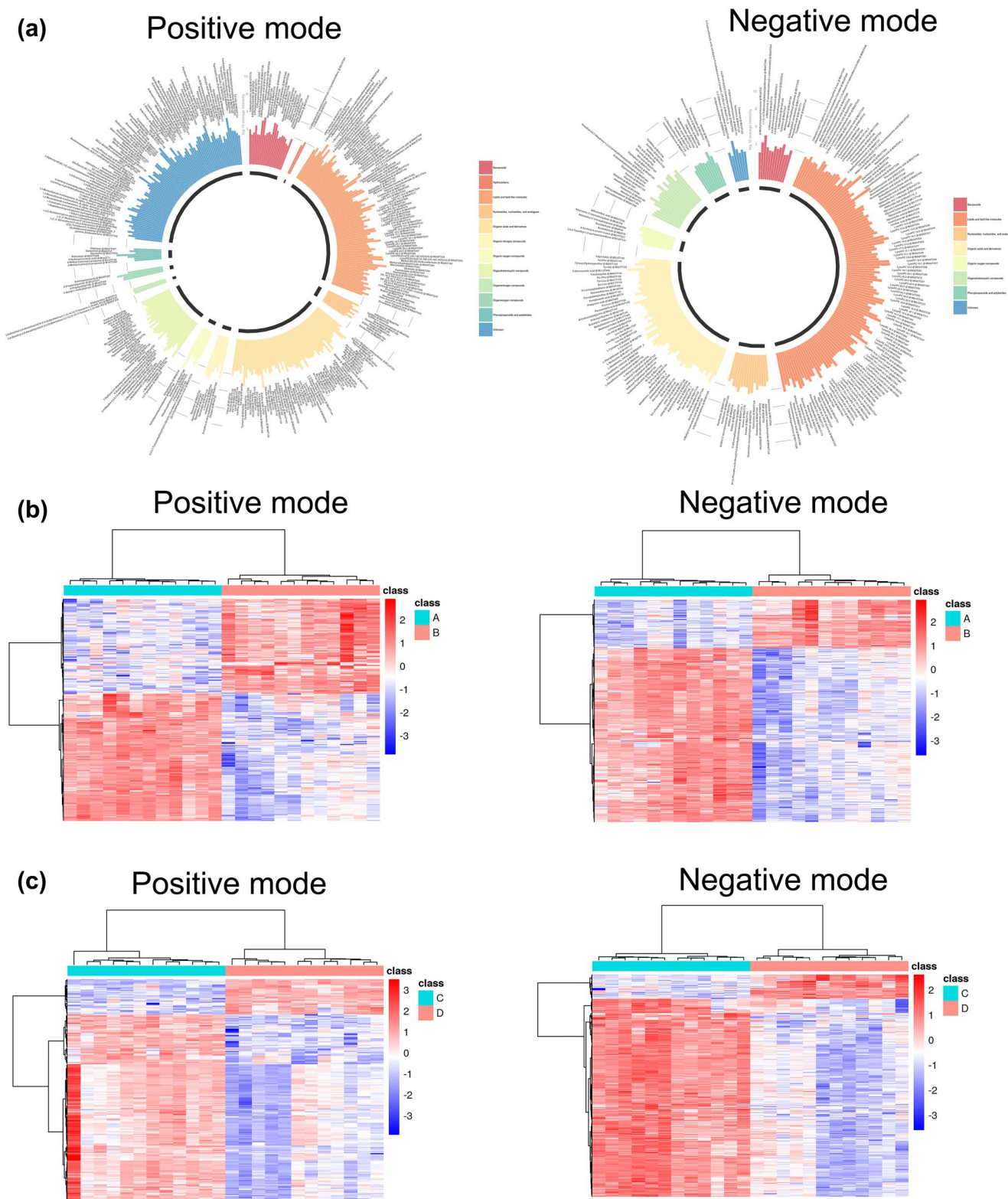## Positive mode

Negative mode

FIGURE 3 Overview of the characteristics of differential metabolites. (a) Molecules related to lipid metabolism and organic acids and their derivatives. The number of unidentifiable metabolites in the negative ion mode is higher than that in the positive ion mode. Different colours represent different metabolite classifications; (b) Heatmaps showing the differential metabolites between the zirconium oxide nanoparticle (ZrO_2 NP) and control groups at 24 h in the positive and negative ion modes; (c) Heatmaps of differential metabolites between the ZrO_2 NP and control groups at 48 h in the positive and negative ion modes. Each line represents a differential metabolite; each box denotes a cell sample; and different colours signify different abundance

TABLE 1 Differential metabolites response to ZrO_2 NPs exposure

Mode	Comparison	All	Up	Down
Pos	B/A	5142	96	129
Neg	B/A	4964	91	326
Pos	D/C	5142	33	174
Neg	D/C	4964	37	302

Note: All, all high-quality features; up, upregulated; down, downregulated; mode, the mode in which the mass spectrometer detects the substance, including positive ion mode (Pos) and negative ion mode (Neg). A: Group A, MC3T3-E1 cells with mock treatment for 24 h. B: Group B, MC3T3-E1 with 100 μg/ml ZrO_2 NPs for 24 h. C: Group C, MC3T3-E1 cells with mock treatment for 48 h. D: Group D MC3T3-E1 with 100 μg/ml ZrO_2 NPs for 48 h as group D.

Abbreviation: ZrO_2 NPs, zirconium oxide nanoparticles.

3.4 | Functional analysis of differential metabolites

A pathway analysis is a useful tool for understanding complex relationships among genes and proteins. First, we used an HMDB analysis (http://www.hmdb.ca/) to study the differential metabolites functions. Considering there was a good separation between the ZrO_2 NPs-treated and control groups in the negative ion mode, we focussed on the negative ion mode. The findings indicated that the differential metabolites were mainly lipids and lipid-like molecules at 48 h following ZrO_2 NP treatment in the negative ion mode (Figure 4a,b).

To further analyse the metabolic pathways associated with ZrO_2 NP toxicity, we conducted a KEGG pathway analysis. The results revealed that the differential metabolites following ZrO_2 NP treatment for 24 h in the negative ion mode were enriched in metabolic pathways and glycerophospholipid metabolism (Figure 4c). The differential metabolites following ZrO_2 NP treatment for 48 h in the negative ion mode were enriched in metabolic pathways and glycerophospholipid metabolism (Figure 4d). They had a good consistency, which indicates that ZrO_2 NP exposure to MC3T3-E1 cells has an important influence on the cell membrane system.

3.5 | Identification of potential metabolite biomarkers

Multivariate statistical analysis of VIP values obtained from PLS-DA was performed to identify the metabolites with the greatest contribution to cell classification at 24 and 48 h following ZrO_2 NP treatment. The criteria for selecting candidate metabolites as biomarkers were (1) ratio ≥ 2 or ratio $\leq 1/2$; (2) p-value ≤ 0.05; (3) VIP ≥ 1. The PLS-DA plot showed a separation of metabolites, with the greatest contribution to cell classification occurring between Group A and Group B (Figure 5a) and Group C and Group D (Figure 5b). Then, combined with univariate statistical analysis including t-test and FC, all metabolites with a significant contribution of $p \leq 0.05$ or FC $\geq 2/\leq 0.5$ were considered to be potential biomarkers. A total of 66 endogenous differential metabolites were identified in the Group B when compared with Group A,

and a total of 67 endogenous differential metabolites were identified in the Group D when compared with Group C. A Venn diagram revealed that 42 endogenous differential metabolites were common in both the 24 and 48 h collections (Figure 5c), most of which were lysoPCs and lysoPEs (Table 2). These differential metabolites may be responsive to ZrO_2 NP exposure and may function as possible biomarkers for ZrO_2 NP-induced MC3T3-E1 injury.

4 | DISCUSSION

The LC-MS metabolome analysis demonstrated that MC3T3-E1 cells treated with ZrO_2 NPs for 24 and 48 h showed different metabolic characteristics from those of the control group. Most of the differential metabolites formed following ZrO_2 NP treatment were lipids and lipid-like molecules, which were enriched in metabolic pathways and glycerophospholipid metabolism. Forty-two differential metabolites were identified as potential biomarkers, and most of them were classified as lysoPCs or lysoPEs. Therefore, we conclude that the metabolites lysoPCs and lysoPEs can be used as potential biomarkers for ZrO_2 NP toxicity and can provide new insight on how to improve ZrO_2 NP dental materials.

Phosphatidylcholine (PC) and phosphatidylethanolamide (PE) both belong to phospholipids, which are the key components of cell membranes. Phosphatidylcholine and phosphatidylethanolamide are desaturated into lysoPCs (products of PC by phospholipase A1) and lysoPEs, which are important for the synthesis of plasmalogens. Plasmalogens are antioxidants that play a critical role in preventing damage caused by oxidation imbalance. Therefore, reduced levels of lysoPCs and lysoPEs lead to increased oxidative stress [16, 17]. When used in a cell culture medium, lysoPCs induce cell proliferation, transduce intracellular signals, and inhibit apoptosis [18, 19]. LysoPCs also reduce infiltration of immune cells into the lungs and play an anti-inflammatory role by activating the peroxisome proliferator-activated receptor [20, 21]. It has been reported that reduced lysoPCs contribute to a variety of diseases, such as diabetes, vascular diseases, cancers, and depression [22–26]. A quantitative analysis of lysoPCs under pathological conditions is important for understanding their downstream signalling pathways and pathological mechanisms [22–26]. Furthermore, lysoPEs inhibit inflammation by blocking TGF-β1/Smad2/3 signalling and modulating mitochondria-mediated oxidative stress and apoptosis [27, 28]. These studies indicate that lysoPCs and lysoPEs can be used as biomarkers for the early diagnosis and prediction of disease outcome. Indeed, lysoPCs have already been considered as potential biomarkers for diagnosing diabetes in its early stage [29, 30]. Lysophosphatidylcholines have also shown potential in cancer diagnosis. Several lysoPCs were found to be decreased in lung cancer patients [31].

In this study, we established that the levels of lysoPCs (including LysoPC 20:3, LysoPC 22:6, LysoPC 20:2, LysoPC 18:1, LysoPC 16:0, LysoPC 16:1, LysoPC 18:2) and lysoPEs
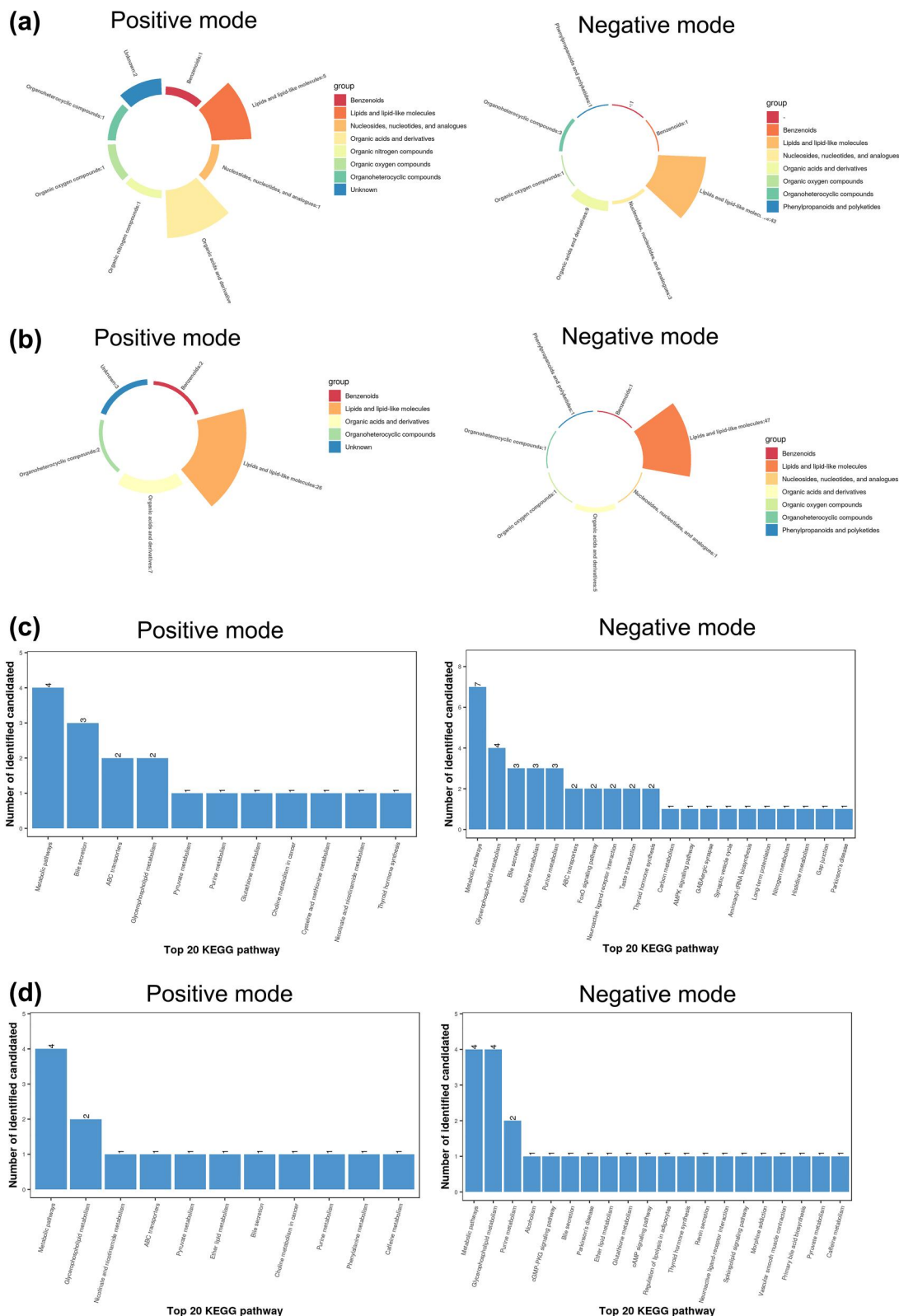
FIGURE 4 Secondary identification and functional analysis of differential metabolites. (a) Secondary identification of differential metabolites following a 24 h zirconium oxide nanoparticle (ZrO$_2$ NP) treatment; (b) Kyoto Encyclopedia of Genes and Genomes (KEGG) pathway analysis of differential metabolites following a 24 h ZrO$_2$ NP treatment; (c) Secondary identification of differential metabolites following a 48 h ZrO$_2$ NP treatment; (d) KEGG pathway analysis of differential metabolites following a 48 h ZrO$_2$ NP treatment
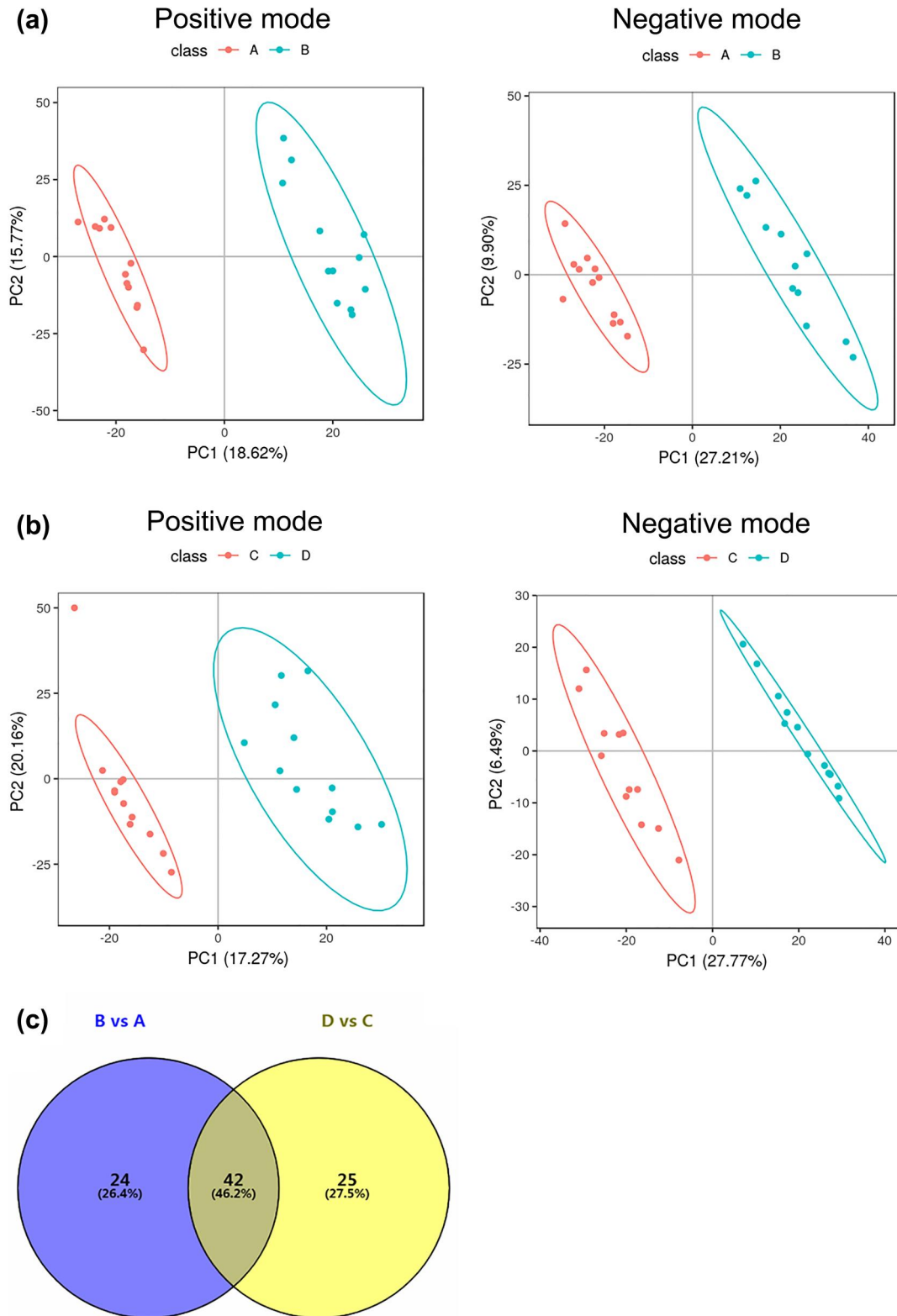
FIGURE 5 Identification of candidate metabolites as potential markers. (a) partial least squares-discriminant analysis partial least squares discriminant analysis (PLS-DA) plot presenting separation of metabolites, with the greatest contribution to cell classification occurring between the zirconium oxide nanoparticles (ZrO$_2$ NPs)-treated and control groups at 24 h; (b) PLS-DA plot showing separation of metabolites, with the greatest contribution to cell classification occurring between the ZrO$_2$ NPs-treated and control groups at 48 h; (c) Venn diagram illustrating the endogenous differential metabolites common to groups treated with ZrO$_2$ NPs for 24 and 48 h

T A B L E 2 Metabolites derived from the pairwise PLS-DA models

ID	Metabolite	VIP	p value	Regulated	Superclass
M319T310	18-Hydroxyeicosatetraenoic acid	4.144667	8.28×10^{-9}	Down	Lipids and lipid-like molecules
M474T209	LysoPE 18:3	2.801086	1.85×10^{-5}	Down	Lipids and lipid-like molecules
M137T56	1-Methylnicotinamide	2.783056	0.000413966	Down	Organoheterocyclic compounds
M611T95	L-Glutathione (oxidised form)	2.762714	8.19×10^{-7}	Down	Organic acids and derivatives
M504T267	LysoPE 20:2	2.70355	8.40×10^{-5}	Down	Lipids and lipid-like molecules
M167T237	Phthalic acid	2.702434	1.33×10^{-7}	Down	Benzenoids
M498T205	LysoPE 20:5	2.682045	4.89×10^{-7}	Down	Lipids and lipid-like molecules
M611T62_3	Glutathione, oxidised	2.603731	2.21×10^{-6}	Down	Organic acids and derivatives
M590T247	LysoPC 20:3	2.554472	2.75×10^{-6}	Down	Lipids and lipid-like molecules
M450T211	LysoPE 16:1	2.553959	7.84×10^{-6}	Down	Lipids and lipid-like molecules
M544T245	LysoPS 20:4; LysoPS 20:4	2.53665	6.93×10^{-5}	Down	Lipids and lipid-like molecules
M612T222	LysoPC 22:6	2.528219	9.56×10^{-7}	Down	Lipids and lipid-like molecules
M506T257	Plasmenyl-PE 20:0; PE(P-16:0/4:0)	2.499394	1.73×10^{-5}	Down	Lipids and lipid-like molecules
M592T272	LysoPC 20:2	2.482021	1.90×10^{-6}	Down	Lipids and lipid-like molecules
M566T257	LysoPC 18:1	2.458142	9.56×10^{-7}	Down	Lipids and lipid-like molecules
M436T257	PE(P-16:0e/0:0)	2.443241	1.02×10^{-5}	Down	Lipids and lipid-like molecules
M277T238	Mono-2-ethylhexyl phthalate	2.408902	5.42×10^{-6}	Down	Benzenoids
M538T217	LysoPC 16:1	2.356646	1.94×10^{-6}	Down	Lipids and lipid-like molecules
M586T206	LysoPC 20:5	2.346388	4.31×10^{-7}	Down	Lipids and lipid-like molecules
M552T246	LysoPC 17:1	2.303782	0.000118428	Down	Lipids and lipid-like molecules
M522T285	LysoPS 18:1; LysoPS 18:1	2.298806	4.81×10^{-6}	Down	Lipids and lipid-like molecules
M502T245	LysoPE 20:3	2.277507	8.72×10^{-5}	Down	Lipids and lipid-like molecules
M536T204	LysoPC 16:2	2.19811	2.07×10^{-7}	Down	Lipids and lipid-like molecules
M594T308	LysoPC 20:1	2.18754	5.21×10^{-6}	Down	Lipids and lipid-like molecules
M540T245	LysoPC 16:0	2.178957	3.83×10^{-5}	Down	Lipids and lipid-like molecules
M588T222	LysoPC 20:4	2.144495	6.36×10^{-6}	Down	Lipids and lipid-like molecules
M506T303	LysoPE 20:1	2.059453	9.73×10^{-5}	Down	Lipids and lipid-like molecules
M618T286	LysoPC 22:3	2.047479	0.000143077	Down	Lipids and lipid-like molecules
M564T228	LysoPC 18:2	2.027778	5.58×10^{-5}	Down	Lipids and lipid-like molecules
M452T235	LysoPE 16:0	2.00022	0.000215468	Down	Lipids and lipid-like molecules
M512T206	LysoPC 14:0	1.968704	3.49×10^{-5}	Down	Lipids and lipid-like molecules
M580T281	LysoPC 19:1	1.94714	5.78×10^{-6}	Down	Lipids and lipid-like molecules
M448T202	LysoPE 16:2	1.921952	0.001360486	Down	Lipids and lipid-like molecules
M299T298	2-Hydroxystearate	1.919112	8.60×10^{-6}	Down	Lipids and lipid-like molecules
M524T259	Glycocholic acid	1.884938	3.25×10^{-5}	Down	Lipids and lipid-like molecules
M524T220	LysoPE 22:6	1.82143	0.000107996	Down	Lipids and lipid-like molecules
M500T221	LysoPE 20:4	1.805229	6.21×10^{-5}	Down	Lipids and lipid-like molecules
M496T267	LysoPS 16:0; LysoPS 16:0	1.78735	0.000107288	Down	Lipids and lipid-like molecules
M614T230	LysoPC 22:5	1.784389	0.000165904	Down	Lipids and lipid-like molecules

(Continues)

T A B L E 2 (Continued)

ID	Metabolite	VIP	p value	Regulated	Superclass
M570T245	LysoPS 22:5; LysoPS 22:5	1.717136	0.022280103	Down	Lipids and lipid-like molecules
M378T105	S-Lactoylglutathione	1.650778	0.005595764	Down	Organic acids and derivatives
M319T137	Asn-Trp	4.064022	4.25×10^{-7}	Up	Organic acids and derivatives

Abbreviation: PLS-DA, partial least squares discriminant analysis.

(including LysoPE 20:3 and LysoPE 20:1), were significantly reduced in MC3T3-E1 cells treated with ZrO_2 NPs, which indicates that lysoPCs and lysoPEs could be potential biomarkers for ZrO_2 NP toxicity. Particularly, evidence has shown that there is an association between the levels of lysoPCs and lysoPEs [32]. Therefore, we should consider a combined detection of lysoPCs and lysoPEs to improve the diagnostic accuracy.

Previous studies have revealed that the treatment of MC3T3-E1 cells with ZrO_2 NPs for 48 h caused more severe changes in the cell morphology and stronger inhibition of cell differentiation than the treatment for 24 h [13]. In this study, 66 and 67 endogenous differential metabolites were identified in the group treated with ZrO_2 NPs for 24 and 48 h, respectively. Our results indicate that ZrO_2 NPs have more severe cytotoxic effects after long-term exposure compared to that of short-term exposure. However, exposure to ZrO_2 NPs for 24 and 48 h both resulted in changes in the levels of lysoPCs and lysoPEs, which suggests that lysoPCs and lysoPEs are effective biomarkers for both short- and long-term exposure to ZrO_2 NPs.

The limitation of our study is that a metabolomic analysis is only the first step. A detailed assessment of combined lysoPCs and lysoPEs as biomarkers in the diagnosis of ZrO_2 NP toxicity is still lacking. Therefore, further analysis on the clinical application of combined lysoPCs and lysoPEs is necessary. Nevertheless, the results in the present study will provide new sights into diagnostic approaches for ZrO_2 NP toxicity and how to improve ZrO_2 NP dental materials to reduce the risk of injury to the cell membrane system.

In conclusion, we have identified different metabolic characteristics in MC3T3-E1 cells treated with ZrO_2 NPs for 24 and 48 h. Our study provides new evidence supporting lysoPCs and lysoPEs as potential biomarkers for the diagnosis of cytotoxicity of ZrO_2 NPs and offers insight on how ZrO_2 NP dental materials can be improved to reduce the risk of cell membrane system injury.

ORCID
Mingfu Ye https://orcid.org/0000-0001-9564-2142

REFERENCES
1. Shimazaki, M., et al.: Metastable zirconia phases prepared from zirconium alkoxide and yttrium acetylacetonate: part 1–formation and characterization of metastable zirconia solid solutions. Mater. Res. Bull. 28(9), 878–884 (1993)
2. Ju-Nam, Y., Lead, J.R.: Manufactured nanoparticles: an overview of their chemistry, interactions and potential environmental implications. Sci. Total Environ. 400(1–3), 396–414 (2008)
3. Arefian, Z., et al.: Potential toxic effects of zirconia oxide nanoparticles on liver and kidney factors. Biomed. Res. 26(1), 89–97 (2015)
4. Zhao, J., Castranova, V.: Toxicology of nanomaterials used in nanomedicine. J. Toxicol. Environ. Health B Crit. Rev. 14(8), 593–632 (2011)
5. Ha, S.W., Weitzmann, M.N., Beck, G.R., Jr.: Bioactive silica nanoparticles promote osteoblast differentiation through stimulation of autophagy and direct association with Lc3 and P62. ACS Nano. 8(6), 5898–5910 (2014)
6. Nel, A., et al.: Toxic potential of materials at the nanolevel. Science. 311(5761), 622–627 (2006)
7. Kepp, O., Galluzzi, L., Kroemer, G.: Mitochondrial control of the Nlrp3 inflammasome. Nat. Immunol. 12(3), 199–200 (2011)
8. Sorbara, M.T., Girardin, S.E.: Mitochondrial ROS fuel the inflammasome. Cell Res. 21(4), 558–560 (2011)
9. Zhang, T., et al.: Identification of potential biomarkers for ovarian cancer by urinary metabolomic profiling. J. Proteome Res. 12(1), 505–512 (2013)
10. Buesen, R., et al.: Effects of SiO_2, ZrO_2, and $BaSO_4$ nanomaterials with or without surface functionalization upon 28-day oral exposure to rats. Arch. Toxicol. 88(10), 1881–1906 (2014)
11. Lindeque, J.Z., et al.: Metabolomics reveals the depletion of intracellular metabolites in Hepg2 cells after treatment with gold nanoparticles. Nanotoxicology. 12(3), 251–262 (2018)
12. Xie, J., et al.: Research on the hepatotoxicity mechanism of citrate-modified silver nanoparticles based on metabolomics and proteomics. Nanotoxicology. 12(1), 18–31 (2018)
13. Ye, M., Shi, B.: Zirconia nanoparticles-induced toxic effects in osteoblast-like 3t3-E1 cells. Nanoscale Res. Lett. 13(1), 353 (2018)
14. Yu, C., et al.: Comparative metabolomics reveals the metabolic variations between two endangered Taxus species (T. Fuana and T. Yunnanensis) in the Himalayas. BMC Plant Biol. 18(1), 197 (2018)
15. Wen, B., et al.: Metax: a flexible and comprehensive software for processing metabolomics data. BMC Bioinf. 18(1), 183 (2017)
16. Li, M., et al.: Emodin opposes chronic unpredictable mild stress induced depressive-like behavior in mice by upregulating the levels of hippocampal glucocorticoid receptor and brain-derived neurotrophic factor. Fitoterapia. 98, 1–10 (2014)
17. Mao, Q.Q., et al.: Peony glycosides produce antidepressant-like action in mice exposed to chronic unpredictable mild stress: effects on hypothalamic-pituitary-adrenal function and brain-derived neurotrophic factor. Prog. Neuro-Psychopharmacol. Biol. Psychiatry. 33(7), 1211–1216 (2009)
18. Wang, C., Wang, M., Han, X.: Comprehensive and quantitative analysis of lysophospholipid molecular species present in obese mouse liver by shotgun lipidomics. Anal. Chem. 87(9), 4879–4887 (2015)
19. Wang, M., et al.: Novel advances in shotgun lipidomics for biology and medicine. Prog. Lipid Res. 61, 83–108 (2016)

20. Knuplez, E., et al.: Lysophosphatidylcholines inhibit human eosinophil activation and suppress eosinophil migration in vivo. Biochim. Biophys. Acta Mol. Cell Biol. Lipids. 1865(7), 158686 (2020)

21. Klingler, C., et al.: Lysophosphatidylcholines activate pparδ and protect human skeletal muscle cells from lipotoxicity. Biochim. Biophys. Acta. 1861(12 Pt A), 1980–1992 (2016)

22. Razquin, C., et al.: Plasma lipidomic profiling and risk of type 2 diabetes in the PREDIMED trial. Diabetes Care. 41(12), 2617–2624 (2018)

23. Schmitz, G., Ruebsaamen, K.: Metabolism and atherogenic disease association of lysophosphatidylcholine. Atherosclerosis. 208(1), 10–18 (2010)

24. Kühn, T., et al.: Higher plasma levels of lysophosphatidylcholine 18:0 are related to a lower risk of common cancers in a prospective metabolomics study. BMC Med. 14, 13 (2016)

25. Wu, Y., et al.: Quantitative proteomics analysis of the liver reveals immune regulation and lipid metabolism dysregulation in a mouse model of depression. Behav. Brain Res. 311, 330–339 (2016)

26. Liu, H., et al.: Study on a Dspe-Lc-Ms/Ms method for lysophosphatidylcholines and underivatized neurotransmitters in rat brain tissues. J. Chromatogr. B Analyt. Technol. Biomed. Life Sci. 1096, 11–19 (2018)

27. Pathil, A., et al.: Ursodeoxycholyl lysophosphatidylethanolamide attenuates hepatofibrogenesis by impairment of Tgf-B1/Smad2/3 signalling. Br. J. Pharmacol. 171(22), 5113–5126 (2014)

28. Wang, J., et al.: Ursodeoxycholyl lysophosphatidylethanolamide protects against hepatic ischemia and reperfusion injury in mice. Shock. 43(4), 379–386 (2015)

29. Hu, C., Wang, M., Han, X.: Shotgun lipidomics in substantiating lipid peroxidation in redox biology: methods and applications. Redox Biol. 12, 946–955 (2017)

30. Lauritano, C., et al.: Lysophosphatidylcholines and chlorophyll-derived molecules from the diatom cylindrotheca closterium with anti-inflammatory activity. Mar. Drugs. 18(3), 166 (2020)

31. Dong, J., et al.: Lysophosphatidylcholine profiling of plasma: discrimination of isomers and discovery of lung cancer biomarkers. Metabolomics. 6(4), 478–488 (2010)

32. Lin, M., et al.: Lipidomics as a tool of predicting progression from non-alcoholic fatty pancreas disease to type 2 diabetes mellitus. RSC Adv. 9, 41419–41430 (2019)